ASTROBIOLOGY
Volume 13, Number 6, 2013

DOI: 10.1089/ast.2012.0817

Abiotic Production of Methane in Terrestrial Planets

Andrés Guzmán-Marmolejo,[1] Antígona Segura,[2,3] and Elva Escobar-Briones[4]

Abstract

On Earth, methane is produced mainly by life, and it has been proposed that, under certain conditions, methane detected in an exoplanetary spectrum may be considered a biosignature. Here, we estimate how much methane may be produced in hydrothermal vent systems by serpentinization, its main geological source, using the kinetic properties of the main reactions involved in methane production by serpentinization. Hydrogen production by serpentinization was calculated as a function of the available FeO in the crust, given the current spreading rates. Carbon dioxide is the limiting reactant for methane formation because it is highly depleted in aqueous form in hydrothermal vent systems. We estimated maximum CH_4 surface fluxes of 6.8×10^8 and 1.3×10^9 molecules cm^{-2} s^{-1} for rocky planets with 1 and 5 $M_\oplus$, respectively. Using a 1-D photochemical model, we simulated atmospheres with volume mixing ratios of 0.03 and 0.1 CO_2 to calculate atmospheric methane concentrations for the maximum production of this compound by serpentinization. The resulting abundances were 2.5 and 2.1 ppmv for 1 $M_\oplus$ planets and 4.1 and 3.7 ppmv for 5 $M_\oplus$ planets. Therefore, low atmospheric concentrations of methane may be produced by serpentinization. For habitable planets around Sun-like stars with N_2-CO_2 atmospheres, methane concentrations larger than 10 ppmv may indicate the presence of life. Key Words: Serpentinization—Exoplanets—Biosignatures—Planetary atmospheres. Astrobiology 13, 550–559.

1. Introduction

Missions such as EChO (Tessenyi *et al.*, 2012) and the James Webb Space Telescope (Deming *et al.*, 2009) may be able to detect atmospheric compounds from potentially habitable planets around other stars. With Earth as the only known habitable planet, the ongoing question is how to distinguish a habitable planet from an inhabited one, having a single template, Earth, for establishing the characteristics of habitable exoplanets. In the present paper, we will call habitable planets those which meet the general conditions of being rocky, with water, massive enough to retain their atmospheres, and with an average surface temperature above the freezing point of water (*e.g.*, Kasting and Catling, 2003; Segura and Kaltenegger, 2010). Our analysis is constrained to anoxic atmospheres because the most stable bulk atmospheric composition of an abiotic rocky planet is CO_2 and N_2, as is the case of early Earth (*e.g.*, Zahnle *et al.*, 2010), Mars, and Venus.

To detect life on a planet, global changes to the planetary surface or atmosphere must have occurred due to the presence of a biota. For example, chemical compounds produced by life may be abundant enough to produce a signature in the planetary spectrum. The spectral features of this type of molecule are called biological signatures or biosignatures (Des Marais *et al.*, 2002; Kaltenegger *et al.*, 2002; Meadows, 2006).

Oxygen (O_2) and ozone (O_3) are signals of life in Earth's atmosphere; O_2 is produced by photosynthesis, while O_3 is generated by O_2 photolysis. On habitable planets around Sun-like stars, high CO_2 atmospheres do not produce high-enough abiotic O_2 or O_3 to be detected in the planetary spectrum (Segura *et al.*, 2007). Consequently, they are usable biosignatures for terrestrial planets (Des Marais *et al.*, 2002).

Methane (CH_4) has also been proposed as another possible biosignature (Des Marais *et al.*, 2002). Nevertheless, CH_4 can be produced by both biological and geological sources. Biological CH_4 is generated by methanogenic bacteria from

$$CO_2 + 4H_2 \rightarrow CH_4 + 2H_2O \qquad \text{(R1)}$$

$$CH_3CO_2H \text{ (or any other small organic compounds)} \rightarrow CH_4 + CO_2$$

Experimental simulations of hydrothermal vent environments have shown that methane forms abiotically in these systems (*e.g.*, McCollom and Seewald, 2001; Oze *et al.*, 2012).

[1]Instituto de Geofísica, Universidad Nacional Autónoma de México, Ciudad Universitaria, México.
[2]Instituto de Ciencias Nucleares, Universidad Nacional Autónoma de México, Ciudad Universitaria, México.
[3]Member of the Virtual Planetary Laboratory, a NASA Astrobiology Institute lead team.
[4]Instituto de Ciencias del Mar y Limnología, Universidad Nacional Autónoma de México, Ciudad Universitaria, México.

These results agree with the detection of methane on peridotite-dominated hydrothermal vents in which methanogens are not present (*e.g.*, Proskurowski *et al.*, 2006; Fiebig *et al.*, 2007). Abiotic production of methane is usually explained by a reaction of Fischer-Tropsch synthesis (*e.g.*, McCollom *et al.*, 1999; Charlou *et al.*, 2002; Fiebig *et al.*, 2007), where H_2 molecules reduce CO_2, forming CH_4, as in Reaction R1. Hydrogen for this reaction comes from the process known as serpentinization, which will be detailed in the next section.

There are no atmospheric processes that yield CH_4 in CO_2- or O_2-rich atmospheres. The sinks for atmospheric CH_4 are (1) in O_2-poor atmospheres, CH_4 is broken by photolysis below 145 nm, which leads to the production of CH_3, CH_2, and CH radicals (Atreya *et al.*, 2006); (2) in O_2-rich atmospheres, CH_4 reacts quickly with the hydroxyl radical (OH) through the following reactions:

$$O_2 + h\nu(\lambda < 200\ \text{nm}) \rightarrow :O + :O$$
$$:O + O_2 \rightarrow O_3$$
$$O_3 + h\nu\ (\lambda < 310\ \text{nm}) \rightarrow O_2 + O^*$$
$$O^* + H_2O \rightarrow 2\cdot OH$$
$$CH_4 + \cdot OH \rightarrow \cdot CH_3 + H_2O$$

The removal of atmospheric CH_4 from O_2-rich atmospheres is faster and more efficient than the geological production rate, so these atmospheres need a biological source to maintain high CH_4 concentrations. For this reason, some authors such as Lovelock (1965), Sagan *et al.* (1993), and Des Marais *et al.* (2002) have suggested that CH_4 detection, together with O_2 (or O_3), would be good evidence of life. However, this rule may not apply for planets with high O_2 atmospheres around M dwarfs, where methane can build up because of the particular UV emission from these stars (Segura *et al.*, 2005). In abiotic, CO_2-rich atmospheres, CH_4 may be detectable in the planetary spectrum even if its source is solely geological (Segura *et al.*, 2007). With the aim to evaluate the relevance of methane as a biosignature in terrestrial planets, we estimated possible production rates of methane from serpentinization processes. Then we used the production rates to evaluate CH_4 fluxes and the atmospheric abundances in terrestrial CO_2-rich atmospheres, using a 1-D photochemical model coupled to a 1-D climate model.

2. Abiotic Methane Production

Methane can be produced by serpentinization. Through this process, Fe- and Mg-rich ultramafic rocks, like olivine, are transformed to serpentine ($Mg_3Si_2O_5(OH)_4$) by hydrolysis. Other products are brucite ($Mg(OH)_2$), magnetite (Fe_3O_4), and H_2. Serpentinization occurs in hydrothermal vent systems at mid-ocean ridges (*e.g.*, Proskurowski *et al.*, 2006) and subduction zones (*e.g.*, Hyndman and Peacock, 2003). It is a complex process that may be described by the following reaction sequence (Bach *et al.*, 2006):

$$2Mg_{1.8}Fe_{0.2}SiO_4 + 3H_2O \leftrightarrow$$
$$1Mg_{2.85}Fe_{0.15}Si_2O_5(OH)_4 + 1Mg_{0.75}Fe_{0.25}(OH)_2 \quad \text{(R2)}$$
$$57Mg_{0.75}Fe_{0.25}(OH)_2 + 30SiO_{2(aq)} \leftrightarrow$$
$$15Mg_{2.85}Fe_{0.15}Si_2O_5(OH)_4 + 23H_2O + 4Fe_3O_4 + 4H_2 \quad \text{(R3)}$$
$$3Mg_{0.9}Fe_{0.1}SiO_3 + 2H_2O \leftrightarrow Mg_{2.7}Fe_{0.3}Si_2O_5(OH)_4 + SiO_{2(aq)} \quad \text{(R4)}$$

During serpentinization, H_2 is formed at the mineral surface as a result of the Fe^{2+} oxidation. This reaction needs aqueous silica that is likely to be provided by the breakdown of orthopyroxene to serpentine (Bach *et al.*, 2006). Indeed, serpentinization has been proposed as an abundant H_2 source (McCollom and Seewald, 2001; Sleep *et al.*, 2004). In environments with abundant CO_2, CH_4 is formed from rising $H_{2(aq)}$ generated by serpentinization (Reaction R1). This occurs at ridges in the seafloor associated with hydrothermal vent flows (pH 9–11).

2.1. Abundance of reactants for CH_4 abiotic production in terrestrial planets

2.1.1. Iron abundance. Iron (FeO) is consumed during serpentinization, and the renewal of the crust by plate tectonics provides new Fe^{2+} that can be used in the serpentinization process. The oceanic crust composition is nearly homogeneous, with FeO content between 6 and 10 wt % (Taylor and McLennan, 1985; Condie, 1997) and a density of 3×10^6 g m^{-3}. Then the FeO abundance in the oceanic crust is 2.5×10^3 and 4.2×10^6 mol m^{-3}, for 6 and 10 wt %, respectively. FeO is supplied as new crust forms, with a production rate that can be expressed as

$$Fe_{(m)} = C_n \rho f_{FeO} \quad (1)$$

where ρ is the crust density, f_{FeO} is the iron mass fraction in the crust, and C_n is the crust formation rate calculated as $C_n = l\times d\times S_c$, with l the total length of the ridges, d the average thickness of the crust, and S_c the crust spreading rate. Table 1 shows the values used for the 1 $M_\oplus$ planet and those estimated for the 5 $M_\oplus$ planet. The values for the 5 $M_\oplus$ planet were scaled from Earth by using the power law $M_m = bm^x$, with M_m a given variable (*e.g.*, crust thickness, ridge length) for a planet with m Earth masses, b Earth's value for that variable, and x the exponent calculated by Valencia *et al.* (2007a). The crust density and the iron fraction were assumed to be equal to Earth's values.

The iron supply rate is then calculated to be between 9.1×10^{12} and 1.5×10^{13} mol yr^{-1} for 1 $M_\oplus$ planets and between 4.7×10^{13} and 7.8×10^{13} for 5 $M_\oplus$ planets. The minimum and maximum supply rates correspond to crust FeO mass fraction contents of 0.06 and 0.1, respectively.

2.1.2. Hydrogen production. In a strict sense, serpentinization is described by Reactions R2 to R4, although it is usually expressed from its redox state, controlled by the

Table 1. Planet Parameters for Calculating FeO Formation Rates

Variable	*Exponent*	*1* $M_\oplus$[a]	*5* $M_\oplus$[b]
Ridge length (l)	0.28	7×10^7 m	1.1×10^8 m
Crust thickness (d)	−0.45	2600 m	1260.2 m
Spreading rate (S_c)	1.19	2 cm yr^{-1}	13.6 cm yr^{-1}

[a]Total length of the ridges and average crustal thickness from Macdonald (2001), average spreading rate sustained on Earth during the last ~150 million years (Cogné and Humler, 2004, and references therein).
[b]Calculated from Valencia *et al.* (2007a); see text.

quartz-fayalite-magnetite buffer, represented by equilibrium in the aqueous fluid for the reaction (Basaltic Volcanism Study Project, 1981)

$$3Fe_2SiO_4 + 2H_2O \leftrightarrow 2Fe_3O_4 + 3SiO_2 + 2H_{2(aq)} \quad (R5)$$

From this, we can assume a simple reaction between a solid A and a liquid phase B, where the reaction velocity is $v_r = \kappa[A]^x$, where κ is the kinetic rate constant, A is the fayalite concentration, and x is the reaction order (Rudge *et al.,* 2010). Here, we assume that R5 is a first-order reaction for fayalite, so that $v_r = \kappa[Fe_2SiO_4]$. From the R5 stoichiometry, the H_2 reaction velocity $vf(H_2) = 2v_r$, so that $vf(H_2) = 2\kappa[Fe_2SiO_4]$. To use the FeO values calculated before, we will express the fayalite abundance by its FeO equivalent content ($2[Fe_2SiO_4] = [FeO]$), so that $vf(H_2) = \kappa[FeO]$.

The rate constant κ has not been experimentally evaluated for R5 but was parameterized by Kelemen and Matter (2008) from volumetric studies of peridotite hydrolysis (Martin and Fyfe, 1970) as

$$\kappa = \kappa_0 \left(\frac{a_0}{a}\right)^2 e^{-\alpha(T-T_0)^2} \quad (2)$$

where a is the fayalite grain size, T is the reaction temperature, and κ_0, a_0, α, and T_0 are the constants given in Table 2. The H_2 formation rate [$vf(H_2)$] can then be calculated from the FeO abundance, temperature, and grain size. Maximum H_2 formation rate is reached at 260°C. Such a temperature is possible if we consider that serpentinization occurs in hydrothermal vent systems where the temperature varies from 40°C to 400°C (*e.g.,* Kelley *et al.,* 2005; Haase *et al.,* 2009).

The contact area between the mineral surface and the liquid phase depends on the grain size a. For this parameter, the optimum value for maximizing $vf(H_2)$ is 70 μm. As we mentioned in Section 2.1.1, the FeO supply ($Fe_{(m)}$) depends on the creation of new crust that has rates of 9.1×10^{12} and 4.7×10^{13} FeO mol yr^{-1}, for 1 and 5 $M_\oplus$ planets, respectively.

To verify the balance between the generated and consumed FeO, we consider the reaction

$$3FeO + H_2O \rightarrow Fe_3O_4 + H_2 \quad (R6)$$

From the Reaction R6 stoichiometry, we can establish a relationship between the formation rates of FeO ($Fe_{(m)}$) and H_2. If $3vf(H_2) > Fe_{(m)}$, all the FeO will be consumed, and the reaction would happen only during a given period of time. If $3vf(H_2) < Fe_{(m)}$, the reaction could continue indefinitely. When $3vf(H_2) = Fe_{(m)}$, the H_2 formation is in equilibrium with the generation of FeO, and the reaction is at a sustainable limit. Because $vf(H_2) = \kappa[FeO]$, then $3\kappa[FeO] = Fe_{(m)}$. Then, using the values for the grain size and temperature that optimize κ and the maximum rates for FeO production, we obtain $[FeO] = 26.4$ mol m^{-3}. This FeO abundance is available under the conditions assumed here (see Section 2.1.1). Then the maximum production of H_2 is 3.0×10^{12} mol yr^{-1} (1.1×10^{10} molecules cm^{-2} s^{-1}) for a 1 $M_\oplus$ planet and 1.6×10^{13} mol yr^{-1} (2.2×10^{10} molecules cm^{-2} s^{-1}) for a 5 $M_\oplus$ planet.

Table 2. Values for Calculation of the Parameterization of the Serpentinization Constant Rate

Constant	*Value*
κ_0	1×10^{-6} s^{-1}
a_0	70 μm
α	2.09×10^{-4} °C^{-2}
T_0	260°C

2.1.3. Carbon dioxide abundance. On Earth, CO_2 is recycled in the atmosphere-crust system by tectonic activity. It is estimated that the preindustrial ocean intake was $\sim6.2\times10^{15}$ mol CO_2 yr^{-1}, from which only 1.7×10^{13} mol CO_2 yr^{-1} form carbonates (Siegenthaler and Sarmiento, 1993). Sedimentary carbon is estimated to be 7.1×10^{21} mol (Holser *et al* 1988) to 7.75×10^{21} mol (Hirschmann and Dasgupta, 2009), equivalent to ~62–68 bar of atmospheric CO_2, respectively. Of this volume, 15–20% by mole is organic carbon, and the remaining 80–85% is carbonate (Holser *et al.,* 1988). A review by Hirschmann and Dasgupta (2009) of CO_2 estimations in the mantle gives a range of $\sim9.75\pm4.2\times10^{21}$ mol with the mid value equivalent to ~85 bar of atmospheric CO_2. The CO_2 production in the mid-ocean ridge was calculated to be 2.2×10^{12} mol yr^{-1} (Marty and Tolstikhin, 1998) and more recently $9.3\pm2.8\times10^{11}$ mol yr^{-1} (Fischer, 2008).

Two possible sources of CO_2 may then be available for reacting with H_2 to form methane (R1) in the hydrothermal vent systems. One source comes directly from the mantle and may be the most likely for oceanic crust spreading centers; the other source is the decarboxylation of carbonates in sediments. Carbonates, mainly in the form of calcite, release CO_2 at temperatures above 500°C (Morse *et al.,* 2007). This means that they can be a relevant source of CO_2 only if they are deep enough in the crust to reach those temperatures. Therefore, carbonate decarboxylation may be an important source of CO_2 for hydrothermal vent systems associated with subduction zones, like back-arc systems. Regardless of the high amount of carbon in the mantle and crust, aqueous CO_2 is quantitatively depleted in hydrothermal vent systems. The largest CO_2 concentrations measured in hydrothermal vents are 3×10^3 mol m^{-3} in the Mariana Arc (Sakai *et al.,* 1990). This concentration is 100 times larger than those measured on most of the hydrothermal vent systems located in the mid-ocean ridge (Lupton *et al.,* 2006). The aqueous CO_2 supersaturation found in the Mariana Arc is only explained if there is a source of liquid CO_2 (Brewer *et al.,* 1999, 2000, 2002) leaking into the hydrothermal vent flux (Lupton *et al.,* 2006). Lupton *et al.* (2006, 2008) concluded that, for hydrothermal vent systems, the maximum concentration of CO_2 in aqueous phase is 50 mol m^{-3}. This is derived from the water/rock ratio that usually ranges from 1 to 5 for hydrothermal vent systems but can be as large as 12 (Kawahata and Scott, 1990). Aqueous CO_2 concentrations larger than 50 mol m^{-3} require water/rock ratios significantly less than 1, which is both physically and chemically unreasonable for hydrothermal vents.

Even if larger amounts of CO_2 were available in hydrothermal vent systems, recent experiments show that the addition of large amounts of inorganic carbon into hydrothermal serpentinization systems does not enhance abiotic CH_4 production. This is because of the competition of Fe^{2+} incorporation into carbonate solid phases versus

oxidative magnetite formation, which plays an important role in governing the H_2 and CH_4 production (Jones *et al.*, 2010).

3. Methane Production by Serpentinization

Using the program SUPCRT92 (Johnson *et al.*, 1992), we calculated the equilibrium constants (K) for the reactions that produce methane (R1) and H_2 (R5) as a function of temperature (Fig. 1). The equilibrium constant (K) is a measure of the conversion of reactants to products. The equilibrium constants in Fig. 1 show that the formation of H_2 is more efficient at high temperatures, while methane formation is more efficient at low temperatures.

The equilibrium constant can be expressed as a function of the chemical species that participate in the reaction. For R1,

$$K = \frac{[CH_4]_{eq}}{[H_2]_{eq}^4[CO_2]_{eq}} \tag{3}$$

Because we assume that the reaction occurs in water, its concentration is not modified during the reaction, and it is therefore omitted in Eq. 3.

The amounts of the chemical species involved in the reaction change from their initial concentrations $[H_2]_0$, $[CO_2]_0$, and $[CH_4]_0$ to the equilibrium concentrations $[H_2]_{eq}$, $[CO_2]_{eq}$, and $[CH_4]_{eq}$ depending on the limiting reactant in the following form:

(1) If H_2 is the limiting reactant, the initial conditions are $[CO_2]_0 > 0.25[H_2]_0$ and $[CH_4]_0 = 0$. When equilibrium is achieved, the amounts of H_2 and CO_2 consumed are $x[H_2]_0$ and $0.25x[H_2]_0$, respectively, and methane is $0.25x[H_2]_0$, where x is the reaction yield. Then, for each reactant, the equilibrium concentration is equal to the initial concentration minus the consumed amount, and by using the appropriate stoichiometry the product is equal to what was consumed. Then, for this case, $[H_2]_{eq} = [H_2]_0 - x[H_2]_0$, $[CO_2]_{eq} = [CO_2]_0 - 0.25x[H_2]_0$, and $[CH_4]_{eq} = 0.25x[H_2]_0$.

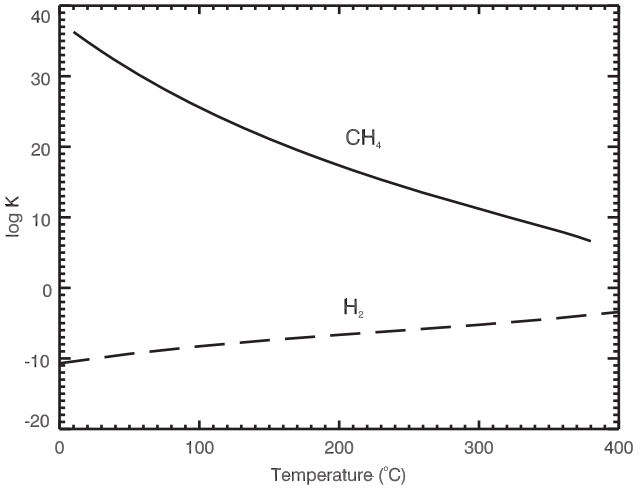

FIG. 1. Equilibrium constant for the production of methane (solid line) and for the production of H_2 (dashed line) as a function of temperature.

(2) If CO_2 is the limiting reactant, then $[CO_2]_0 < 0.25[H_2]_0$ and $[CH_4]_0 = 0$. Consumed H_2 and CO_2 are $4x[CO_2]_0$ and $x[CO_2]_0$, respectively, and the produced methane is $x[CO_2]_0$. At equilibrium, $[H_2]_{eq} = [H_2]_0 - 4x[CO_2]_0$, $[CO_2]_{eq} = [CO_2]_0 - x[CO_2]_0$, and $[CH_4]_{eq} = x[CO_2]_0$.

Substituting the equilibrium quantities on Eq. 3 for both cases:

$$K = \frac{0.25x[H_2]_0}{([H_2]_0(1-x))^4([CO_2]_0 - 0.25x[H_2]_0)} \quad \text{for } H_2 \text{ as limiting reactant} \tag{4}$$

$$K = \frac{x[CO_2]_0}{([H_2]_0 - 4x[CO_2]_0)^4[CO_2]_0(1-x)} \quad \text{for } CO_2 \text{ as limiting reactant} \tag{5}$$

In these equations, K is known, as well as the initial conditions for the reactants, so that the reaction yield x can be calculated as a function of temperature. For H_2, the initial concentration is 3.0×10^{12} mol yr^{-1} for 1 $M_\oplus$ planets and 1.6×10^{13} mol yr^{-1} for 5 $M_\oplus$ planets (see Section 2.1.2). For CO_2, the maximum value is 50 mol m^{-3} (see Section 2.1.3), and assuming a water/rock ratio equal to 1, the amount of rock will be equal to the generated crust volume, that is, 3.6×10^9 m^3 yr^{-1} and 1.9×10^{10} m^3 yr^{-1} for 1 and 5 $M_\oplus$ planets, respectively. The CO_2 available to produce methane then is 1.8×10^{11} mol yr^{-1} for 1 $M_\oplus$ planets and 9.5×10^{11} mol yr^{-1} for 5 $M_\oplus$ planets. For these amounts of H_2 and CO_2, the limiting reactant is CO_2; then we use Eq. 5 to estimate that $x \sim 1$.

Finally, we obtain that for a 1 $M_\oplus$ planet the maximum CH_4 flux is 6.8×10^8 molecules cm^{-12} s^{-1} (1.8×10^{11} mol yr^{-1}), the H_2 flux is 8.6×10^9 molecules cm^{-2} s^{-1} (2.3×10^{12} mol yr^{-1}), and the CO_2 flux is 0.7 molecules cm^{-2} s^{-1} (182 mol yr^{-1}). For the 5 $M_\oplus$ planet, the maximum CH_4 flux is 1.3×10^9 molecules cm^{-2} s^{-1} (9.4×10^{11} mol yr^{-1}), the H_2 flux is 1.7×10^{10} molecules cm^{-2} s^{-1} (1.2×10^{13} mol yr^{-1}), and the CO_2 flux is 1.3 molecules cm^{-2} s^{-1} (939.8 mol yr^{-1}).

Because of the low solubility of methane, we assume that it is released into the atmosphere after it is generated in the hydrothermal vents. Methane could in principle undergo other chemical processes in the ocean, like the formation of methane clathrates, but it is beyond the scope of this work to make a detailed model of the fate of methane in an anoxic ocean. Our assumption is consistent with finding an upper limit for the amount of abiotic methane that may be present in the anoxic atmosphere of a habitable planet.

4. Atmospheric Models

We used two atmospheric models, a 1-D photochemical model (1D-Pm) originally developed by Pavlov and Kasting (2002) that was later modified by Kharecha *et al.* (2005) and Segura *et al.* (2007), and a 1-D radiative/convective model (R-Cm) (Haqq-Misra *et al.*, 2008). The R-Cm produces a temperature profile for an atmosphere with a given bulk atmospheric composition (CO_2, CH_4, and H_2O), and this temperature profile is used as an input for the 1D-Pm.

4.1. Photochemical model

The 1D-Pm computes the chemical equilibrium for 38 chemical species involved in 162 reactions. The atmosphere is divided into 100 layers with a fixed vertical extent of 1 km each. The long-lived chemical species are O, O_2, O_3, H_2O, H, OH, HO_2, H_2O_2, H_2, CO, CO_2, HCO, H_2CO, CH_4, CH_3, C_2H_6, NO, NO_2, HNO, SO, SO_2, and H_2SO_4; N_2 is also included with a constant mixing ratio. The 1D-Pm solves the flux (Eq. 6) and continuity (Eq. 7) equations at each height for each long-lived species, including transport by eddy and molecular diffusion:

$$\Phi_i = -Kn\frac{\partial f_i}{\partial z} - D_i n_i\left(\frac{1}{n_i}\frac{\partial n_i}{\partial_z} + \frac{1}{H_i} + \frac{1+\alpha_{T_i}}{T}\frac{\partial T}{\partial z}\right) \quad (6)$$

$$\frac{\partial n_i}{\partial_t} = p_i - e_i n_i - \frac{\partial f_i}{\partial z} \quad (7)$$

where f_i = flux of the i^{th} species, n_i = number density of the i^{th} species (cm^{-3}), Φ_i = mixing ratio of the i^{th} species, n = total number density of the atmosphere (cm^{-3}), z = altitude (cm), p_i = chemical production rate (cm^{-3} s^{-1}), e_i = chemical loss rate (s^{-1}), and K = eddy diffusion coefficient (cm^{-2} s^{-1}), D_i = diffusion coefficient between species i and the background atmosphere, H_i ($=kT/m_i g$) is the scale height of species i, and α_{Ti} is the thermal diffusion coefficient of species i with respect to the background atmosphere. In these definitions, k = Boltzmann's constant, m_i = molecular mass of species i, and m = molecular mass of the atmosphere.

Boundary conditions for each chemical species were applied at the top and bottom of the model atmosphere, and the resulting set of coupled differential equations was integrated in time to reach a steady state by using the reverse Euler method. The model simulates the Sun's influence over terrestrial anoxic atmospheres, with a fixed solar zenith angle of 50°. A key feature of the 1D-Pm is its ability to keep track of the atmospheric hydrogen (or redox) budget. This is done by considering that when one species is oxidized, another one must be reduced, and vice versa. Following the Kasting and Brown (1998) strategy, "redox-neutral" species are defined as H_2O (for H), N_2 (for N), CO_2 (for C), and SO_2 (for S). All other species are assigned redox coefficients relative to these gases by determining how much H_2 is produced or consumed during their formation from redox neutral species (Appendix 1 in Kharecha *et al.*, 2005). For example, the redox coefficients of CH_4 and NO are calculated from the reactions that would convert them to their corresponding neutral constituents, CO_2 and N_2, respectively:

$$CH_4 + 2H_2O \rightarrow CO_2 + 4H_2$$
$$NO + H_2 \rightarrow \tfrac{1}{2}N_2 + H_2O$$

Then, 1 mol of CH_4 produces 4 mol of H_2, and 1 mol of NO consumes 1 mol of H_2, so that the redox coefficients of CH_4 and NO are +4 and −1, respectively. The contribution of each chemical species i to the hydrogen budget is calculated as $[\Phi_{rain}(i) - \Phi_{surf}(i)]\ H_{coeff}(i)$, where $\Phi_{rain}(i)$ is the loss of species i for rain removal, $\Phi_{surf}(i)$ is the flux from (positive) or into (negative) the ocean of species i, and $H_{coeff}(i)$ is the redox coefficient of that chemical species. The total contributions for loss and production of H_2 are

$$\Phi_{loss} = \sum_i (\Phi_{rain}(i) - \Phi_{surf}(i))H_{coeff}(i) \quad \text{for species with } H_{coeff}(i) < 1 \quad (8)$$

$$\Phi_{prod} = \sum_i (\Phi_{rain}(i) - \Phi_{surf}(i))H_{coeff}(i) \quad \text{for species with } H_{coeff}(i) > 1 \quad (9)$$

The total hydrogen outgassing contribution to the redox budget is expressed as

$$\Phi_{volc}(H_2) = \Phi(H_2) + F(CH_4) \quad (10)$$

For our case, $\Phi(H_2)$ and $F(CH_4) = 4\Phi(CH_4)$ are the fluxes calculated from serpentinization. Then, the hydrogen budget is calculated as

$$\Phi_{volc}(H_2) + \Phi_{prod} = \Phi_{esc}(H_2) + \Phi_{loss} \quad (11)$$

where $\Phi_{esc}(H_2)$ is limited by the H_2 diffusion rate through the homopause. The diffusion-limited escape flux at the top of the atmosphere is calculated using the formulation of Walker (1977) as

$$\Phi_{esc}(H_2) = (b/H) f_{tot}(\text{molecules cm}^{-2}\text{s}^{-1}) \quad (12)$$

where b is an average binary diffusion coefficient for the diffusion of H, H_2, and CH_4 in nitrogen; H is the atmospheric scale height; and f_{tot} is the sum of the mixing ratios at 100 km of all the hydrogen-bearing species abundant in the stratosphere, weighted by the number of hydrogen atoms contained by each of the species (Segura *et al.*, 2007):

$$f_{tot} = f(H_2) + 0.5f(H) + 2f(CH_4)$$

The redox balance in Eq. 11 is diagnostic, not prognostic; hence, it provides a good check both on the redox balance and on the photochemical scheme.

The upper boundary conditions are constant effusion velocity (v_{eff}) or constant flux (Φ_{up}), and for most of the species $v_{eff} = 0$. The flux at the top is expressed as $\Phi_{up} = v_{eff}\ n_i$, where n_i is the number density of the compound i at the top of the atmosphere. For H and H_2, v_{eff} is set equal to the diffusion-limited value, $v_{eff} = D_i/H$. Species such as O_2 that can be photodissociated above the model grid are given upward velocities that balance the column-integrated loss above this level, that is, $v_{eff} = J(O_2)H$, where $J(O_2)$ is the O_2 photolysis rate. Atomic O is then given a fixed downward flux equal to twice the upward flux of O_2. Likewise, photolysis of CO_2 above the model grid leads to downward fluxes of CO and O.

The code has three options for lower (surface) boundary conditions: fixed surface flux, fixed surface mixing ratio, and fixed deposition velocity. Soluble species are removed by direct deposition at the lower boundary to account for the uptake by the ocean. This is done by calculating the flux into the ocean of the chemical species i as $n_i v_{dep}(i)$, with n_i the number density of species i and $v_{dep}(i)$ its deposition velocity. The upper limit on v_{dep} is set by diffusion through the turbulent atmospheric boundary layer, assuming that

Table 3. Parameters for Atmospheric Simulations

			Surface flux (cm^{-2} s^{-1})		*Surface mixing ratio*	
Planet mass	*CO_2 mixing ratio*	T_{surf} *(K)*	*CH_4*	*H_2*	*CH_4*	*H_2*
1 $M_\oplus$	0.03	303.5	6.8×10^{8}	8.6×10^{9}	2.5×10^{-6}	4.7×10^{-4}
	0.1	308.3			2.1×10^{-6}	4.5×10^{-4}
5 $M_\oplus$	0.03	314.2	1.3×10^{9}	1.7×10^{10}	4.1×10^{-6}	4.5×10^{-4}
	0.1	320.5			3.7×10^{-6}	4.6×10^{-4}

molecules are absorbed by the surface each time they collide with it (Kharecha *et al.,* 2005).

4.2. Radiative/Convective model

The R-Cm code is a 1-D cloud-free model with a (log pressure) grid extended from the assumed surface pressure down to a pressure that was set depending on the planetary atmosphere. The program subdivides this range into 101 levels. The time-stepping procedure and the solar (visible/near-IR) portion of the radiation code are from the model of Pavlov *et al.* (2000). The solar code incorporates a δ two-stream scattering algorithm (Toon *et al.,* 1989) to calculate the net absorbed visible and mid IR solar radiation by using four-term, correlated-*k* coefficients to parameterize absorption by O_3, CO_2, H_2O, O_2, and CH_4 in each of 38 spectral intervals (Kasting and Ackerman, 1986). Fluxes in the mid IR are calculated with the hemispheric mean two-stream approximation (Toon *et al.,* 1989). Absorption coefficients in the mid and far IR for methane are those derived by Haqq-Misra *et al.* (2008). All gases other than H_2O are considered to be well mixed in the model atmosphere. A moist adiabatic lapse rate is assumed in the model troposphere with a fixed relative humidity following Manabe and Wetherald (1967).

4.3. Simulated atmospheres

We simulated anoxic atmospheres of lifeless, habitable planets with mixing ratios of 0.03 and 0.1 CO_2. Two planet sizes were tested: 1 $M_\oplus$ and 5 $M_\oplus$; a radius of 1.6 $R_\oplus$ for the 5 $M_\oplus$ planet was calculated by using the mass-radius relationship of Valencia *et al.* (2007b) for a rocky planet (with a

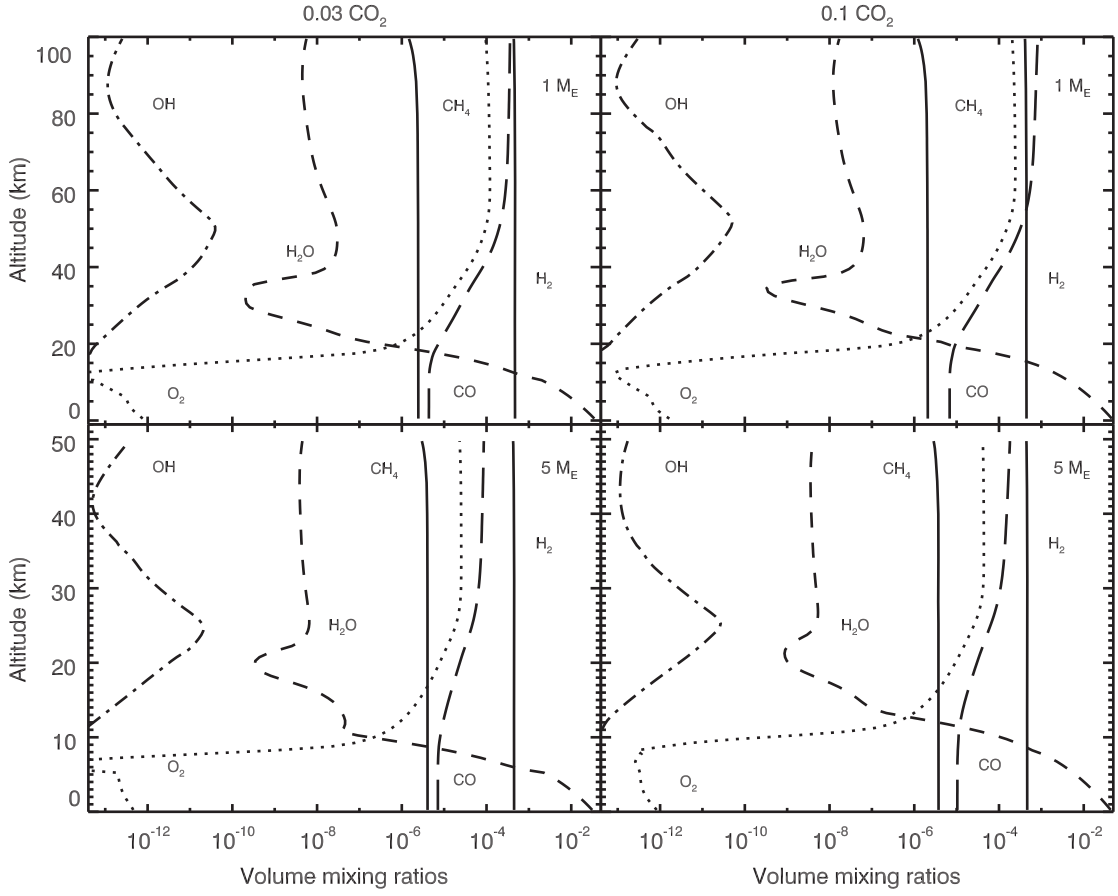

FIG. 2. Mixing ratios of the most relevant chemical species for the simulated atmospheres.

Table 4. Redox Budget for the Simulated Atmospheres (see Text Eqs. 8–12)

		1 $M_\oplus$		5 $M_\oplus$	
Compound	H_{coeff}	*0.03 CO_2*	*0.1 CO_2*	*0.03 CO_2*	*0.1 CO_2*
H_2 production					
H	0.5	5.208×10^{5}	4.762×10^{5}	1.398×10^{5}	1.491×10^{5}
CO	1.0	-2.389×10^{2}	1.426×10^{2}	-2.169×10^{1}	-8.026×10^{1}
HCO	1.5	3.663×10^{6}	5.996×10^{6}	6.843×10^{6}	1.372×10^{7}
H_2CO	2.0	2.760×10^{7}	6.595×10^{7}	8.302×10^{7}	4.980×10^{8}
CH_3	3.5	2.642×10^{6}	1.573×10^{6}	5.067×10^{6}	2.380×10^{6}
C_2H_6	7.0	-1.009	6.819×10^{-2}	-2.734×10^{-2}	-9.842×10^{-2}
SO	1.0	5.647×10^{6}	4.956×10^{6}	5.537×10^{6}	4.271×10^{6}
Φ_{prod}		4.007×10^{7}	7.895×10^{7}	1.006×10^{8}	5.185×10^{8}
Reduced volcanic species					
H_2	1.0	4.477×10^{1}	-5.501	-8.141	9.493
$F(CH_4)$	4.0	2.270×10^{9}	2.720×10^{9}	5.200×10^{9}	5.200×10^{9}
$\Phi(H_2)$		8.600×10^{9}	8.600×10^{9}	1.700×10^{10}	1.700×10^{10}
Φ_{volc}		1.132×10^{10}	1.132×10^{10}	2.220×10^{10}	2.220×10^{10}
Total H_2 production		1.136×10^{10}	1.140×10^{10}	2.230×10^{10}	2.272×10^{10}
H_2 loss					
O	−1.0	-3.699×10^{3}	-6.927×10^{3}	-8.931×10^{2}	-2.201×10^{3}
O_2	−2.0	-5.196×10^{3}	-1.103×10^{4}	-6.057×10^{3}	-1.073×10^{4}
OH	−0.5	-1.977×10^{3}	-1.452×10^{3}	-1.366×10^{3}	-1.203×10^{3}
HO_2	−1.5	-1.173×10^{3}	-4.673×10^{3}	-2.513×10^{3}	-1.217×10^{4}
H_2O_2	−1.0	-2.273	-2.483×10^{3}	-2.026	-6.825
O_3	−3.0	-6.048×10^{-4}	-2.404×10^{-3}	-2.998×10^{-4}	-1.353×10^{-3}
NO	−1.0	-3.798×10^{2}	-7.982×10^{2}	-1.200×10^{2}	-3.769×10^{2}
NO_2	−2.0	-3.734×10^{-4}	-4.720×10^{-3}	-9.372×10^{-5}	-5.896×10^{-2}
HNO	−0.5	-1.408×10^{8}	-2.457×10^{8}	-1.929×10^{8}	-4.368×10^{8}
H_2SO_4	−1.0	-1.099×10^{5}	-1.656×10^{5}	-8.891×10^{4}	-6.232×10^{5}
SO_{4AER}	−1.0	-1.116×10^{8}	-7.708×10^{7}	-1.934×10^{8}	-1.167×10^{8}
Φ_{loss}		-2.525×10^{8}	-3.230×10^{8}	-3.863×10^{8}	-5.541×10^{8}
$\Phi_{esc}(H_2)$		1.144×10^{10}	1.153×10^{10}	2.216×10^{10}	2.217×10^{10}
Total H_2 loss		1.170×10^{10}	1.186×10^{10}	2.255×10^{10}	2.272×10^{10}
H_2 balance		2.875×10^{-2}	3.850×10^{-2}	1.087×10^{-2}	1.748×10^{-4}

similar Fe/Si ratio to Earth) with a 10% water content. The atmospheric surface pressure was scaled with the planet's gravity; therefore, the surface pressures were 1 and 2 bar for the 1 $M_\oplus$ and 5 $M_\oplus$ planets, respectively.

The planets were located at 1.15 AU from the Sun, where the solar flux is 0.75 S_0, with S_0 the solar constant (the flux that is received at the top of the present Earth atmosphere). We choose these atmospheres as illustrative examples of how much methane would exist in the planetary atmosphere given the calculated fluxes of this compound produced by serpentinization. Our choice of stellar distance is the result of considering that (1) closer distances between the planet and the star will mean higher surface temperatures and higher UV stellar fluxes, which are both detrimental to the methane abundance; (2) being near the outer limit of the habitable zone (0.53 S_0, 1.37 AU, Table III in Kasting *et al.*, 1993) requires the inclusion of CO_2 cloud condensation in the R-Cm, a process which is presently not included in the model.

The climate model uses a pressure grid that is "translated" to an altitude grid to transfer the calculated temperature profile to the photochemical model. For the minimum pressures ($\sim10^{-6}$ bar) that the R-Cm code is able to manage, the atmosphere altitudes are $\sim$70 km for planets with 1 $M_\oplus$ and $\sim$35 km for planets with 5 $M_\oplus$. The temperatures above those altitudes were considered constant and equal to the last upper value calculated by the R-Cm. Temperature profiles were calculated by using the Manabe-Wetherald relative humidity profile (Manabe and Wetherald, 1967), with an O_2 mixing ratio of 10^{-15} and no O_3. Carbon dioxide was included by using the selected mixing ratios of 0.03 and 0.1. The first temperature profile was created with a guess value for the CH_4 mixing ratio, and after running the 1D-Pm code to equilibrium, a new temperature profile was calculated with the CH_4 mixing ratio computed by the 1D-Pm code. This process was not repeated unless the change for the methane mixing ratio was larger than a factor of 2.

Boundary surface conditions in the photochemical model were as follows: a fixed deposition velocity for CO, $v_{dep}(CO)=1\times10^{-8}$ cm s^{-1}, and a fixed velocity deposition for H_2 equal to zero; both values are consistent with calculations for an abiotic planet (Kharecha *et al.*, 2005). The methane lower boundary condition was set as a fixed surface flux with the values calculated for maximum production by serpentinization. Table 3 presents the relevant parameters for the modeled atmospheres.

4.4. Abundance of atmospheric methane

Table 3 presents the atmospheric methane abundance obtained for the simulated atmospheres. Mixing ratios obtained by the photochemical model for the most important chemical species are presented in Fig. 2. For all cases,

Table 5. Abundances of Principal Constituents in Hydrothermal Vent Fluxes (Tivey, 2007), Compared with Abundances Calculated by Our Model

	Mid-ocean ridge		*Back-arc basin*		*Rainbow*		*Lost City*	
	Observed	*Our model*	*Observed*	*Our model*	*Observed*	*Our model*	*Observed*	*Our model*
T (°C)	≤405	405	278–334	306	365	365	≤91	91
H_2 (mol m^{-3})	5×10^{-4} to 38	1.3×10^{-2}	0.035–0.5	460	13	8.1	<1–15	1×10^{-7}
CO_2 (mol m^{-3})	3.56–39.9	16.1	14.4–200	1.8×10^{-8}	—	1.9×10^{-8}	—	18.2
CH_4 (mol m^{-3})	7×10^{-3} to 2.58	2.56	$5\times10^{-}$ 10^{-2}	18.8	0.13–2.2	18.7	1–2	0.5

methane was lower than 5 ppmv. The redox budget was conserved in all cases as shown in Table 4.

5. Discussion

Oze *et al.* (2012) proposed that H_2/CH_4 ratios larger than 40 indicate the absence of biological sources of methane based on serpentinization experiments with a water/rock ratio of 2.5 and an analysis of several hydrothermal vent systems with and without methanogens. In our model (H_2/CH_4) ∼ 13, and in order to achieve the ratio proposed by these authors, we need to assume that CO_2 is limited to 18.75 mol m^{-3} instead of 50 mol m^{-3}. This is consistent with the scenario we have proposed, in which CO_2 is the limiting reactant for methane formation, regardless of its abundance in the planetary crust and mantle.

We tested our model by comparing the calculated production of CO_2, H_2, and CH_4 with those measured in hydrothermal vent systems. We used a CO_2 concentration of 18.75 mol m^{-3} given that 50 mol m^{-3} is a maximum that is not usually achieved in Earth's hydrothermal vent systems (see Section 2.1.3). Table 5 shows a comparison between the measured values and our model for CO_2, H_2, and CH_4 in four hydrothermal vent systems. The measured temperature in Table 4 was used as an input for our model. The other parameters used in our model were as follows: 6 wt % FeO in the crust, crust density of 3×10^6 g m^{-3}, grain size of 70 μm, and 26.4 mol m^{-3} available to participate in serpentinization.

The hydrothermal vent systems that are best reproduced by our model are those in the mid-ocean ridge. This is something we expect because we used the average iron abundance measured in those systems. Insular arc systems are mainly found in the west margin of the Pacific Ocean, and they are associated with subduction zones (Pearce and Stern, 2006; Martínez *et al.*, 2007), in which the ocean crust is mainly composed of Si- and Al-rich felsic rocks (Martínez *et al.*, 2007) with low Fe (Le Maitre *et al.*, 2002). The lower Fe content explains the smaller concentration of H_2 in those systems, compared to the ones calculated by the model. The Rainbow system is located at the Southeast of the Azores Islands, over the mid-Atlantic Ridge. This system is lying on an ultramafic rock substratum (Douville *et al.*, 2002) that has more Fe than the average mid-ocean ridge systems. Therefore, larger amounts of H_2 are expected to be produced in these systems.

Previous work has estimated abiotic methane production rates of 10^{12} mol yr^{-1} (∼4×10^9 molecules cm^{-2} s^{-1}) (Kasting and Catling, 2003; Segura *et al.*, 2007). According to our model, the FeO needed to achieve those methane fluxes is 1.4×10^{13} mol yr^{-1}, while Earth only generates 9.1×10^{12} mol yr^{-1}. This means that a methane flux of 10^{12} mol yr^{-1} may not be sustained with the current crust spreading rates.

The results obtained here for the atmospheric abundance of methane may not apply to habitable planets around main sequence M stars (M dwarfs), where the sinks of methane are perturbed due to the particular UV radiation emitted by these stars (Segura *et al.*, 2005). Simulations by Domagal-Goldman *et al.* (2011) for atmospheres with 0.3 CO_2 showed that, for a surface methane flux of 7×10^{10} molecules cm^{-2} s^{-1}, methane atmospheric abundances were ∼3 times larger for planets around M dwarfs than for a planet irradiated by the Sun.

6. Conclusions

The methane production for terrestrial planets was estimated by considering geological processes that occur within hydrothermal vent systems, linked to crust spreading centers, and estimating the kinetic properties of the main reactions involved in CH_4 production by serpentinization. Hydrogen production by serpentinization was calculated as a function of the available FeO in the crust, given the present spreading rates. Carbon dioxide is the limiting reactant for methane formation because it is highly depleted in aqueous form in hydrothermal vent systems. We estimated maximum surface CH_4 fluxes of 6.8×10^8 and 1.3×10^9 molecules cm^{-2} s^{-1} for rocky planets with 1 $M_\oplus$ and 5 $M_\oplus$, respectively. Using a 1-D photochemical model, we simulated poor- and rich-CO_2 atmospheres to calculate atmospheric CH_4 mixing ratios. The resulting abundances were 2.5×10^{-6} and 2.1×10^{-6} for 1 $M_\oplus$ planets and 4.1×10^{-6} and 3.7×10^{-6} for 5 $M_\oplus$ planets.

We have shown that low atmospheric concentrations of methane may be produced by serpentinization. For habitable planets with N_2-CO_2 atmospheres, concentrations of methane larger than 10 ppmv may indicate the presence of life.

Acknowledgments

We thank Norman Sleep and an anonymous referee for their constructive suggestions that greatly improved this work. We acknowledge support from the Universidad Nacional Autónoma de México grant DGAPA PAPIIT IN119709-3. This work was also performed as part of the NASA Astrobiology Institute's Virtual Planetary Laboratory Lead Team, supported by the NASA Astrobiology Institute under Cooperative Agreement Notice NNH05ZDA001C.

Author Disclosure Statement

No competing financial interests exist.

Abbreviations

1D-Pm, 1-D photochemical model; R-Cm, 1-D radiative/convective model.

References

Atreya, S.K., Adams, E.Y., Niemann, H.B., Demick-Montelara, J.E., Owen, T.C., Fulchignoni, M., Ferri, F., and Wilson, E.H. (2006) Titan's methane cycle. *Planet Space Sci* 54:1177–1187.

Bach, W., Paulick, H., Garrido, C.J., Ildefonse, B., Meurer, W.P., and Humphris, S.E. (2006) Unraveling the sequence of serpentinization reactions: petrography, mineral chemistry, and petrophysics of serpentinites from MAR 15°N (ODP Leg 209, Site 1274). *Geophys Res Lett* 33:4–7.

Basaltic Volcanism Study Project. (1981) *Basaltic Volcanism on the Terrestrial Planets,* Pergamon Press, New York.

Brewer, P.G., Friederich, G., Peltzer, E.T., and Orr, F.M.J. (1999) Direct experiments on the ocean disposal of fossil fuel CO_2. *Science* 284:943–945.

Brewer, P.G., Peltzer, E.T., Friederich, G., Aya, I., and Yamane, K. (2000) Experiments on the ocean sequestration of fossil fuel CO_2: pH measurement and hydrate formation. *Mar Chem* 72:83–93.

Brewer, P.G., Peltzer, E.T., Friederich, G., and Rehder, G. (2002) Experimental determination of the fate of rising CO_2 droplets in seawater. *Environ Sci Technol* 36:5441–5446.

Charlou, J.L., Donval, J.P., Fouquet, Y., Jean-Baptiste, P., and Holm, N. (2002) Geochemistry of high H_2 and CH_4 vent fluids issuing from ultramafic rocks at the Rainbow Hydrothermal Field (36°14′N, MAR). *Chem Geol* 191:345–359.

Cogné, J.-P. and Humler, E. (2004) Temporal variation of oceanic spreading and crustal production rates during the last 180 My. *Earth Planet Sci Lett* 227:427–439.

Condie, K.C. (1997). *Plate Tectonics and Crustal Evolution,* Elsevier, Boston.

Deming, D., Seager, S., Winn, J., Miller-Ricci, E., Clampin, M., Lindler, D., Greene, T., Charbonneau, D., Laughlin, G., Ricker, G., Latham, D., and Ennico, K. (2009) Discovery and characterization of transiting super Earths using an all-sky transit survey and follow-up by the James Webb Space Telescope. *Publ Astron Soc Pac* 121:952–967.

Des Marais, D.J., Harwit, M.O., Jucks, K.W., Kasting, J.F., Lin, D.N.C., Lunine, J.I., Schneider, J., Seager, S., Traub, W.A., and Woolf, N.J. (2002) Remote sensing of planetary properties and biosignatures on extrasolar terrestrial planets. *Astrobiology* 2:153–181.

Domagal-Goldman, S.D., Meadows, V.S., Claire, M.W., and Kasting, J.F. (2011) Using biogenic sulfur gases as remotely detectable biosignatures on anoxic planets. *Astrobiology* 11:419–441.

Douville, E.C., Charlou, J.L., Oelkers, E.H., Bienvenu, P., Jove, C.F., Donval, J.P., Fouquet, Y., Prieur, D., and Appriou, P. (2002) The rainbow vent fluids (36°14′N, MAR): the influence of ultramafic rocks and phase separation on trace metal content in Mid-Atlantic Ridge hydrothermal fluids. *Chem Geol* 184:37–48.

Fiebig, J., Woodland, A., Spangenberg, J., and Oschmann, W. (2007) Natural evidence for rapid abiogenic hydrothermal generation of CH_4. *Geochim Cosmochim Acta* 71:3028–3039.

Fischer, T.P. (2008) Fluxes of volatiles (H_2O, CO_2, N_2, Cl, F) from arc volcanoes. *Geochem J* 42:21–38.

Haase, K.M., Petersen, S., Koschinsky, A., Seifert, R., Devey, C.W., Keir, R., Lackschewitz, K.S., Melchert, B., Perner, M., Schmale, O., Süling, J., Dubilier, N., Zielinski, F., Fretzdorff, S., Garbe-Schönberg, C.-D., Westernstroer, U., German, C.R., Shank, T.M., Yoerger, D., Giere, O., Küver, J., Marbler, H., Mawick, J., Mertens, C., Stöber, U., Walter, M., Ostertag-Henning, C., Paulick, H., Peters, M., Strauss, H., Sander, S., Stecher, J., Warmuth, M., and Weber, S. (2009) Fluid compositions and mineralogy of precipitates from Mid Atlantic Ridge hydrothermal vents at 4°48′S. doi:10.1594/PANGAEA.727454.

Haqq-Misra, J.D., Domagal-Goldman, S.D., Kasting, P.J., and Kasting, J.F. (2008) A revised, hazy methane greenhouse for the Archean Earth. *Astrobiology* 8:1127–1137.

Hirschmann, M.M. and Dasgupta, R. (2009) The H/C ratios of Earth's near surface and deep reservoirs, and the consequences for deep Earth volatile cycles. *Chem Geol* 262:4–16.

Holser, W.T., Schidlowski, M., Mackenzie, F.T., and Maynard, J.B. (1988) Geochemical cycles of carbon and sulfur. In *Chemical Cycles in the Evolution of the Earth*, edited by C.B. Gregor, R.M. Garrels, F.T. Mackenzie, and J.B. Maynard, Wiley, New York, pp 105–173.

Hyndman, R.D. and Peacock, S.M. (2003) Serpentinization of the forearc mantle. *Earth Planet Sci Lett* 212:417–432.

Johnson, J.W., Oelkers, E.H., and Helgeson, H.C. (1992) SUPCRT92: A software package for calculating the standard molar thermodynamic properties of minerals, gases, aqueous species, and reactions from 1 to 5000 bar, and 0 to 1000°C. *Comput Geosci* 18:899–947.

Jones, L.C., Rosenbauer, R., Goldsmith, J.I., and Oze, C. (2010) Carbonate control of H_2 and CH_4 production in serpentinization systems at elevated P-Ts. *Geophys Res Lett* 37:1–6.

Kaltenegger, L., Fridlund, M., and Kasting, J.F. (2002) Review on habitability and biomarkers. In *ESA Special Publication: Earth-like Planets and Moons*, edited by B.H. Foing and B. Battrick, ESA Publications Division, Noordwijk, the Netherlands, pp 277–282.

Kasting, J.F. and Ackerman, T.P. (1986) Climatic consequences of very high CO_2 levels in the Earth's early atmosphere. *Science* 234:1383–1385.

Kasting, J.F. and Brown, L.L. (1998) Setting the stage: The early atmosphere as a source of biogenic compounds. In *The Molecular Origins of Life: Assembling the Pieces of the Puzzle*, edited by A. Brack, Cambridge University Press, Cambridge, UK, pp 35–56.

Kasting, J.F. and Catling, D. (2003) Evolution of a habitable planet. *Annu Rev Astron Astrophys* 41:429–463.

Kasting, J.F., Whitmire, D.P., and Reynolds, R.T. (1993) Habitable zones around main sequence stars. *Icarus* 101:108–128.

Kawahata, H. and Scott, S.D. (1990) Strontium isotopes and water-rock interaction of the Agrokipia "B" stockwork deposit in the Troodos ophiolite, Cyprus: a fossil subseafloor ore body. *Geochem J* 24:349–356.

Kelemen, P.B. and Matter, J.M. (2008) *In situ* carbonation of peridotite for CO_2 storage. *Proc Natl Acad Sci USA* 105:17295–17300.

Kelley, D.S., Karson, J.A., Früh-Green, G.L., Dana, R., Yoerger, D.R., Shank, T.M., Butterfield, D.A., Hayes, J.M., Schrenk, M.O., Olson, E.J. Proskurowski, G., Jakuba, M., Bradley, A., Larson, B., Ludwig, K., Glickson, D., Buckman, K., Bradley, A.S., Brazelton, W.J., Roe, K., Elend, M.J., Delacour, A., Bernasconi, S.M., Lilley, M.D., Baross, J.A., Summons, R.E., and Sylva, S.P. (2005) A serpentinite-hosted ecosystem: the Lost City hydrothermal vent field. *Science* 307:1428–1434.

Kharecha, P., Kasting, J.F., and Siefert, J. (2005) A coupled atmosphere–ecosystem model of the early Archean Earth. *Geobiology* 3:53–73.

Le Maitre, R.W., Streckeisen, A., Zanettin, B., Le Bas, M.J., Bonin, B., and Bateman, P. (2002) *Igneous Rocks: A Classification and Glossary of Terms,* Cambridge University Press, Cambridge, UK.

Lovelock, J.E. (1965) A physical basis for life detection experiments. *Nature* 207:568–570.

Lupton, J., Butterfield, D., Lilley, M., Evans, L., Nakamura, K., Chadwick, W., Resing, J., Embley, R., Olson, E., Proskurowski, G., Baker, E., de Ronde, C., Roe, K., Greene, R., Lebon, G., and Young, C. (2006) Submarine venting of liquid carbon dioxide on a Mariana Arc volcano. *Geochemistry, Geophysics, Geosystems* 7:1–20.

Lupton, J., Lilley, M., Butterfield, D., Evans, L., Embley, R., Massoth, G., Christenson, B., Nakamura, K., and Schmidt, M. (2008) Venting of a separate CO_2-rich gas phase from submarine arc volcanoes: examples from the Mariana and Tonga-Kermadec arcs. *J Geophys Res* 113:B08S12.

Manabe, S. and Wetherald, R.T. (1967) Thermal equilibrium of the atmosphere with a given distribution of relative humidity. *Journal of the Atmospheric Sciences* 24:241–259.

Martin, B. and Fyfe, W.S. (1970) Some experimental and theoretical observations on the kinetics of hydration reactions with particular reference to serpentinization. *Chem Geol* 6:185–202.

Martínez, F., Okino, K., Ohara, Y., Reysenbash, A.-L., and Goffredi, S.K. (2007) Back-arc basins. *Oceanography* 20:116–127.

Marty, B. and Tolstikhin, I.N. (1998) CO_2 fluxes from mid-ocean ridges, arcs and plumes. *Chem Geol* 145:233–248.

McCollom, T.M. and Seewald, J.S. (2001) A reassessment of the potential for reduction of dissolved CO_2 to hydrocarbons during serpentinization of olivine. *Geochim Cosmochim Acta* 65:3769–3778.

McCollom, T.M., Ritter, G., and Simoneit, B.R. (1999) Lipid synthesis under hydrothermal conditions by Fischer-Tropsch–type reactions. *Orig Life Evol Biosph* 29:153–166.

Macdonald, K.C. (2001) Seafloor spreading: mid-ocean ridge tectonics. In *Encyclopedia of Ocean Sciences*, edited by J. Steele, S. Thorpe, and K. Turekian, Academic Press, San Diego, pp 1798–1813.

Meadows, V.S. (2006) Modeling the diversity of extrasolar terrestrial planets. In *Direct Imaging of Exoplanets: Science & Techniques,* Proceedings of the 200th colloquium of the International Astronomical Union held in Villefranche sur Mer, France, October 3–7, 2005, edited by C. Aime and F. Vakili, Cambridge University Press, Cambridge, UK, pp 25–34.

Morse, J.W., Arvidson, R.S., and Lüttge, A. (2007) Calcium carbonate formation and dissolution. *Chem Rev* 107:342–381.

Oze, C., Jones, L.C., Goldsmith, J.I., and Rosenbauer, R.J. (2012) Differentiating biotic from abiotic methane genesis in hydrothermally active planetary surfaces. *Proc Natl Acad Sci USA* 109:9750–9754.

Pavlov, A.A. and Kasting, J.F. (2002) Mass-independent fractionation of sulfur isotopes in Archean sediments: strong evidence for an anoxic Archean atmosphere. *Astrobiology* 2:27–41.

Pavlov, A.A., Kasting, J.F., Brown, L.L., Rages, K.A., and Freedman, R. (2000) Greenhouse warming by CH_4 in the atmosphere of early Earth. *J Geophys Res* 105:11981–11990.

Pearce, J.A. and Stern, R.J. (2006) Origin of back-arc basin magmas: trace element and isotope perspectives. In *Back-Arc Spreading Systems: Geological, Biological, Chemical, and Physical Interactions,* edited by D.M. Christie, C.R. Fisher, S.-M. Lee, and S. Givens, American Geophysical Union, Washington, DC, pp 63–86.

Proskurowski, G., Lilley, M.D., Kelley, D.S., and Olson, E.J. (2006) Low temperature volatile production at the Lost City hydrothermal field, evidence from a hydrogen stable isotope geothermometer. *Chem Geol* 229:331–343.

Rudge, J.F., Kelemen, P.B., and Spiegelman, M. (2010) A simple model of reaction-induced cracking applied to serpentinization and carbonation of peridotite. *Earth Planet Sci Lett* 291:215–227.

Sagan, C., Thompson, W.R., Carlson, R., Gurnett, D., and Hord, C. (1993) A search for life on Earth from the Galileo spacecraft. *Nature* 365:715–721.

Sakai, H., Gamo, T., Kim, E.-S., Tsutsumi, M., Tanaka, T., Ishibashi, J., Wakita, H., Yamano, M., and Oomori, T. (1990) Venting of carbon dioxide–rich fluid and hydrate formation in mid-Okinawa Trough backarc basin. *Science* 248:1093–1096.

Segura, A. and Kaltenegger, L. (2010) Search for habitable planets. In *Astrobiology: Emergence, Search and Detection of Life*, edited by V.A. Basiuk, American Scientific Publishers, Stevenson Ranch, CA, pp 341–358.

Segura, A., Kasting, J.F., Meadows, V., Cohen, M., Scalo, J., Crisp, D., Butler, R.A.H., and Tinetti, G. (2005) Biosignatures from Earth-like planets around M dwarfs. *Astrobiology* 5:706–725.

Segura, A., Meadows, V.S., Kasting, J.F., Crisp, D., and Cohen, M. (2007) Abiotic formation of O_2 and O_3 in high-CO_2 terrestrial atmospheres. *Astron Astrophys* 472:665–679.

Siegenthaler, U. and Sarmiento, J.L. (1993) Atmospheric carbon dioxide and the ocean. *Nature* 365:119–125.

Sleep, N.H., Meibom, A., Fridriksson, T., Coleman, R.G., and Bird, D.K. (2004) H_2-rich fluids from serpentinization: geochemical and biotic implications. *Proc Natl Acad Sci USA* 101:12818–12823.

Taylor, S.R. and McLennan, S.M. (1985) *The Continental Crust: Its Composition and Evolution,* Blackwell Scientific Publication, Oxford.

Tessenyi, M., Ollivier, M., Tinetti, G., Beaulieu, J.P., Coudé du Foresto, V., Encrenaz, T., Micela, G., Swinyard, B., Ribas, I., Aylward, A., Tennyson, J., Swain, M.R., Sozzetti, A., Vasisht, G., and Deroo, P. (2012) Characterizing the atmospheres of transiting planets with a dedicated space telescope. *Astrophys J* 746, doi:10.1088/0004-637X/746/1/45.

Tivey, M.K. (2007) Generation of seafloor hydrothermal vent fluids and associated mineral deposits. *Oceanography* 20:50–65.

Toon, O.B., McKay, C.P., Ackerman, T.P., and Santhanam, K. (1989) Rapid calculation of radiative heating rates and photodissociation rates in inhomogeneous multiple scattering atmospheres. *J Geophys Res* 94:16287–16301.

Valencia, D., O'Connell, R.J., and Sasselov, D.D. (2007a) Inevitability of plate tectonics on super-Earths. *Astrophys J* 670:L45–L48.

Valencia, D., Sasselov, D.D., and O'Connell, R.J. (2007b) Detailed models of super-Earths: how well can we infer bulk properties? *Astrophys J* 665:1413–1420.

Walker, J.C.G. (1977) *Evolution of the Atmosphere*, Macmillan, New York.

Zahnle, K., Schaefer, L., and Fegley, B. (2010) Earth's earliest atmospheres. *Cold Spring Harb Perspect Biol* 2, doi: 10.1101/cshperspect.a004895.

Address correspondence to:
Antígona Segura
Instituto de Ciencias Nucleares
Universidad Nacional Autónoma de México
Circuito exterior C.U.
A. Postal 70-543
Coyoacán
C. P. 04510
México D.F.
México

E-mail: antigona@nucleares.unam.mx

Submitted 16 January 2012
Accepted 20 February 2013